

Role of refractive index in metalens performance

ELYAS BAYATI,^{1,*}  ALAN ZHAN,² SHANE COLBURN,¹ MAKSYM VIKTOROVICH ZHELJEZNYAKOV,¹
AND ARKA MAJUMDAR^{1,2} 

¹Department of Electrical and Computer Engineering, University of Washington, Seattle, Washington 98195, USA

²Department of Physics, University of Washington, Seattle, Washington 98195, USA

*Corresponding author: elyasb@uw.edu

Received 7 November 2018; revised 22 January 2019; accepted 22 January 2019; posted 24 January 2019 (Doc. ID 351300); published 14 February 2019

Sub-wavelength diffractive optics, commonly known as metasurfaces, have recently garnered significant attention for their ability to create ultra-thin flat lenses with a high numerical aperture. Several materials with different refractive indices have been used to create metasurface lenses (metalenses). In this paper, we analyze the role of refractive index on the performance of these metalenses. We employ both forward and inverse design methodologies to perform our analysis. We found that, while high-refractive-index materials allow for extreme reduction of the focal length, for moderate focal lengths and numerical aperture (<0.6), there is no appreciable difference in the focal spot size and focusing efficiency for metalenses made of different materials with refractive indices ranging between 1.2 and 3.43 in forward design, and 1.25 and 3.5 in inverse design. © 2019 Optical Society of America

<https://doi.org/10.1364/AO.58.001460>

1. INTRODUCTION

Dielectric metasurfaces, two-dimensional quasi-periodic arrays of subwavelength scatterers, have recently emerged as a promising technology to create ultra-thin, flat, and miniature optical elements [1]. With these sub-wavelength scatterers, metasurfaces shape optical wavefronts, modifying the phase, amplitude, and/or polarization of incident light in transmission or reflection. Many different optical components such as lenses [2,3], focusing mirrors [4], vortex beam generators [5,6], holographic masks [7,8], polarization optics [9,10], and freeform surfaces [11] have been demonstrated using metasurfaces. While the sub-wavelength structuring provides the necessary phase-shift for light manipulation, the material degrees of freedom also play an important role in determining the performance.

Metasurfaces initially relied on deep-subwavelength metallic structures and operated at mid-infrared frequencies [1]. The large absorption loss in metals made it difficult to create high-efficiency metasurface devices in the visible and near-infrared (NIR) wavelengths. This motivated the fabrication of metasurfaces using dielectric materials because of the low optical loss of dielectrics at visible and NIR wavelengths. While initial research focused on higher-index amorphous silicon (Si) [3,4] at NIR wavelengths, recently, materials with a lower refractive index, such as titanium oxide (TiO₂) [12], gallium nitride (GaN) [13], and silicon nitride (SiN) [14,15] have been used to create metasurfaces operating at visible wavelengths. Based on the empirical Moss relation $n^4 \sim 1/E_g$ [16] with refractive index n and the electronic bandgap E_g , we expect that a large optical transparency window necessitates the material refractive index

to be lower. Hence, to create metasurfaces at shorter wavelengths, we have to rely on materials with a lower refractive index. In decreasing the refractive index, however, it is unclear what effect there will be on the device performance. Recently, the efficiency of a periodic meta-grating was analyzed at optical frequency as a function of the material refractive index [17]. The authors reported that for large deflection angles, the efficiency decreases with a lower refractive index, but for low deflection angles, there is no significant difference in the efficiency of transmissive thick meta-gratings made of different materials. While this analysis with periodic structures can help to qualitatively understand the performance of a metasurface lens (metalens) with quasi-periodic arrangements of scatterers [18–20], a systematic and quantitative evaluation of material selection for metalenses is currently lacking. It is unclear what is the minimum required dielectric contrast to achieve high-efficiency and high-numerical-aperture metalenses. Answering this question is vital for understanding the capabilities, limitations, efficiency, and manufacturability of metalenses over a specific wavelength range. We note that the effect of refractive index is explicit in the lens maker's formula [21] for a refractive lens:

$$\frac{1}{f} = (n - 1) \left(\frac{1}{R} - \frac{1}{R'} \right),$$

where f is the focal length, n is the refractive index of the lens, and R and R' are the radii of curvature of the two spherical surfaces of the lens. The angle of refraction, and therefore the focal length, depends on the curvature of the lens surface and the material used to construct the lens. However, for metalenses,

to the best of our knowledge, there is no study or theoretical formula relating the refractive index to the focal length or numerical aperture and the efficiency.

In this paper, we design and analyze metalenses made of materials with a wide range of refractive indices to estimate the relationship between the refractive index and the performance of metalenses. We analyze metalenses operating in the NIR spectral regime ($\lambda = 1550$ nm) in terms of efficiency and full width at half maximum (FWHM). We consider six different dielectric materials: Si ($n = 3.43$) [3], TiO_2 ($n = 2.4$) [12], GaN ($n = 2.3$) [13], SiN ($n = 2.0$) [14,15], SiO_2 ($n = 1.5$) [22], and an artificial material with a refractive index of 1.2. The index range <2 is of particular importance as large-scale printable photonics technology, which is promising for low-cost manufacturing of metasurfaces, requires the refractive index to be near 1.5 [23]. First, we used a forward design technique based on the rigorous coupled-wave analysis (RCWA) [24,25], followed by finite-difference time-domain (FDTD) simulations [3,14]. We compared the focusing efficiency and FWHM at the focal plane as a function of the numerical aperture for different materials. We then employed an inverse electromagnetic design based on the generalized Mie scattering theory and adjoint optimization [26] to calculate the dependence of the metalens performance and FWHM at the focal plane on the refractive indices between 1.25 and 3.5.

2. FORWARD DESIGN METHOD

The main building block of a metalens is a scatterer arranged in a subwavelength periodic lattice (with a period p). Here, we assume the scatterers to be cylindrical pillars, arranged in a square lattice, as shown in Fig. 1. Since we have a sub-wavelength

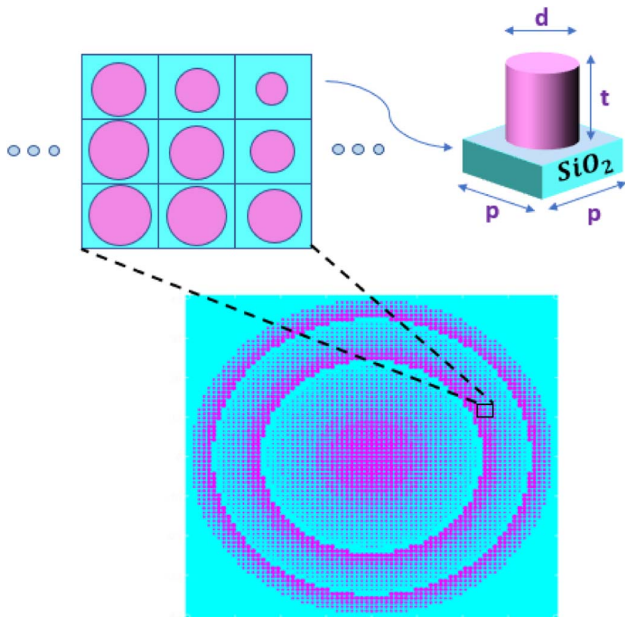


Fig. 1. Schematic of a metalens and its lattice structures. A lattice with periodicity p can be formed using cylindrical pillars (with diameter d and thickness t) on top of a silicon dioxide substrate, arranged in a square lattice. By varying the radius of the cylindrical pillars, we can impart different phase shifts.

periodicity in a metals, only the zeroth-order plane wave propagates a significant distance from the metasurface, and other higher-order diffracted plane waves are evanescent [27]. This makes metalenses more efficient compared to other diffractive optics.

Forward design of a metalens involves selecting the appropriate spatial phase profile for the specific optical component, arranging the scatterers on a subwavelength lattice, and spatially varying their dimensions. To have an arbitrary transmission phase profile, phase shifts of the scatterer should span the 0-to- 2π range, while maintaining large transmission amplitudes. In our simulation, we used the phase profile of metalens as

$$\phi(x, y) = \frac{2\pi}{\lambda} \left(\sqrt{x^2 + y^2 + f^2} - f \right).$$

We discretize this continuous spatial phase profile onto a square lattice with periodicity p , giving us a discrete spatial phase map with different phase values. We then quantize the phase profile with 10 linear steps between 0 and 2π , corresponding to 10 different pillar radii. For each value of this new discrete spatial phase profile, we find the radius of the pillar that most closely reproduces that phase and place it on the lattice.

The complex transmission coefficient of a zeroth-order plane wave depends on the lattice periodicity p , scatterer dimensions (both the diameter d and thickness t), and refractive index n . Using RCWA, we calculate the transmission phase and amplitude of the scatterers as a function of duty cycle (d/p) for different materials assuming a periodic boundary condition (Fig. 2). For different refractive indices, we can find several sets of thickness t and lattice periodicities p that provide a full 0-to- 2π phase shift range under varying diameters while maintaining a high transmission amplitude (transmissivity ~ 1). Some resonant dips in transmission are observed, which can be attributed to guided mode resonances [28]. Metasurface parameters, including lattice periodicity p and thickness t , for each material are shown in Table 1. As we are comparing different materials, we chose these parameters to maintain the same thickness to the period ratio across simulations, in this

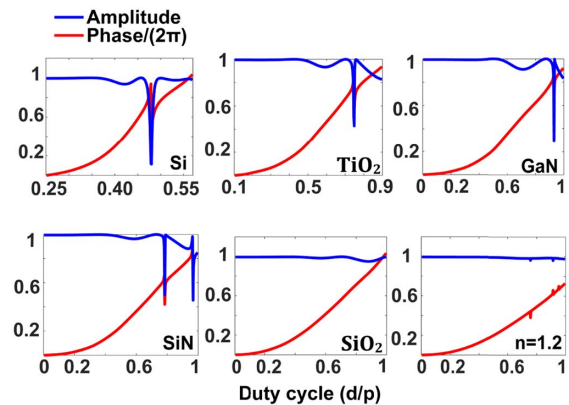


Fig. 2. Amplitude and phase of the transmitted light through a scatterer. Using RCWA, we calculate the transmission properties (red, phase delay; blue, transmission amplitude) as a function of the ratio of the pillar diameter and periodicity. We kept the thickness-to-period ratio, that is, the ratio between the thickness and the periodicity same for all materials, except for $n = 1.2$, to compare their efficiency.

Table 1. Metasurface Parameters Including Lattice Periodicity p and Thickness t for Each Refractive Index Used in the Forward Design Method (Optical Wavelength $\lambda = 1550$ nm)

| Refractive Index (n) | Si ($n = 3.43$) | TiO ₂ ($n = 2.4$) | GaN ($n = 2.3$) | SiN ($n = 2$) | SiO ₂ ($n = 1.5$) | ($n = 1.2$) |
|--------------------------|-------------------|--------------------------------|-------------------|-----------------|--------------------------------|---------------|
| Periodicity (p) (nm) | 775 | 790.5 | 759.5 | 930 | 1372 | 1395 |
| Thickness (t) (nm) | 1240 | 1317 | 1240 | 1550 | 2290 | 5022 |

case selecting $t/p \sim 1.6$. For our artificial material with a refractive index of 1.2, however, to cover the whole 0-to- 2π phase shift range, we need to increase the thickness. To keep the same thickness-to-period ratio, we cannot maintain sub-wavelength periodicity. Hence, for $n = 1.2$, we assume a thickness-to-period ratio of 3.6 to get the maximum possible phase shift. We assume the substrates for all materials to be SiO₂ with a thickness $t_{\text{sub}} = \lambda$. We also note that some of the parameters reported in this paper will be difficult to fabricate. However, in this paper, we primarily want to understand the dependence of the metalens performance on the refractive index, and experimental feasibility is not considered.

Using the parameters obtained from RCWA, we designed arrays of nanopillars and simulated the metalenses using Lumerical FDTD solutions. The pillar diameters corresponding to resonances in Fig. 2 are excluded when designing the metasurfaces to get a higher efficiency. We analyzed the performance of the metalenses in terms of FWHM and focusing

efficiency for different focal lengths (5–200 μm). The diameter of the metalenses is kept constant at 80 μm .

The FWHM of the focal spot is shown in Fig. 3(a) as a function of the numerical aperture, where the solid black curve is the FWHM of a diffraction-limited spot of a lens with the same geometric parameters. More details on the calculation of a diffraction-limited FWHM are presented in Appendix A. There is no appreciable difference in the FWHM across the range of simulated indices, except for $n = 1.2$, where the FWHM does not decrease at very high numerical apertures. We define the focusing efficiency as the power within a radius of three times the FWHM at the focal plane to the total power incident upon the lens [3,14]. Figure 3(b) shows the focusing efficiency as a function of the refractive index of all materials for different numerical apertures. We find that the focusing efficiency decreases with higher numerical apertures, as observed before [3,14]. At low numerical apertures ($\text{NA} < 0.6$), the efficiency of the metalenses is almost independent of the material refractive index. The decrease in the efficiency with increasing numerical aperture, however, is more drastic with a lower refractive index, and the efficiency drops faster in materials with refractive indices below 1.5.

3. INVERSE DESIGN METHOD

In the forward design method, we kept the thickness-to-period ratio (t/p) of the scatterers fixed for different materials. This constraint restricts the design space and makes it difficult to objectively compare metalenses made of different materials. Furthermore, the local phase approximation that we make in going from RCWA to FDTD neglects the coupling between the scatterers. Such coupling is not negligible when the material refractive index is small. We also had to manually inspect the data from RCWA to determine the quality of the parameters and avoid resonant dips before constructing the FDTD simulation. We can circumvent these problems by employing an inverse electromagnetic design methodology developed by our group [26].

Recently, inverse electromagnetic design has been applied to phase profile design [7], single scatterer design [29], beam steering [30], and achromatic metasurface optics [31,32]. We utilize an inverse design method using an adjoint optimization-based gradient descent and the multi-sphere Mie theory, which describes the scattering properties of a cluster of interacting spheres. We determine the interactive scattering coefficients for each sphere individually, similar to what the Mie theory does for a single sphere [33,34]. In our inverse design, we do not make any assumption about the size of our scatterers, but we fix their periodicity. Consequently, we expect to explore a larger design space to find well-suited parameters for our metalenses. Our simulation tool also aims to design the whole

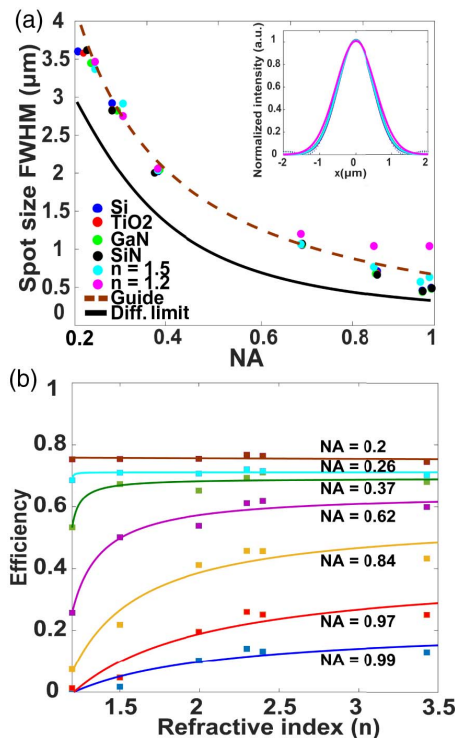


Fig. 3. Performance of the metalens designed using the forward design methodology. (a) The FWHM of the focal spot is plotted as a function of the numerical aperture of the lens. The inset plot of (a) shows a cross section of the beam size for the focal length of 50 μm with their Gaussian fit functions. The solid and dashed curves are the diffraction-limited FWHM and guide to the eye, respectively. (b) The efficiency of metalenses for all materials as a function of the refractive index for each numerical aperture using the forward design method.

metasurface and not just the unit cell, and thus the coupling between scatterers is already included in the design process.

Our inverse design method based on the Mie scattering, however, currently only works for spherical scatterers. Hence, in our design, we optimize the radii of different spheres. The radii and periodicity of the metalenses are chosen to avoid any physical overlap or contact between adjacent spheres. We run the optimization routine up to a fixed number of iterations (in this case 100) to obtain the final metalens. The iteration time of the inverse design method depends on both the particle number and the expansion order of the orbital index l . The expansion order here provides the number of spherical basis functions for each particle to include in our simulation [26]. Larger numbers of particles and expansion orders increase the iteration time. As we are interested in sub-wavelength structures to design metalenses, it is important to find a reasonable cut-off for the expansion order to balance the speed of the iteration and the accuracy of the result. The valid cutoff expansion order (l_{\max}), which is ultimately determined by the physical size and refractive index of the individual spheres relative to the incident wavelength, is chosen to be 3 in our simulations. Since these scattering properties are determined by the geometric and material properties of the sphere, in addition to the wavelength of the incident light, there is a relation between the cutoff expansion order and possible periodicity range of the scatterers. Here, the periodicities of the metalenses are chosen in a way such that the contribution from expansion orders greater than 3 are negligible.

We chose 10 equally spaced refractive indices between 1.25 and 3.5 for the inverse design. We assume a square periodic lattice, where the spheres with different radii are placed. For all simulations, we assume the spheres are suspended in vacuum, and do not include a substrate. Initially, all the spheres have identical radii. We then allow the sphere radii to vary continuously between 150 nm and half of the periodicity to optimize the figure of merit, which is the intensity at the designed focal point. The periodicities for all refractive indices for the inverse design method are shown in Table 2. The final radii distribution of the optimization process for one metalens using inverse design method is shown in Fig. 4. We find that the result is mostly rotationally symmetric as expected for a lens. We attribute the slight asymmetry near the origin to our optimization running for a fixed number of iterations and converging at a local minimum. The radius of the designed metalenses is 20 μm , and five focal lengths between 15 and 100 μm are tested to provide us the same number of numerical apertures for better comparison with forward design.

Table 2. Periodicity Values for 10 Different Refractive Indices Used in the Inverse Design Method

| Refractive Index (n) | Periodicity (p) (nm) | Refractive Index (n) | Periodicity (p) (nm) |
|--------------------------|--------------------------|--------------------------|--------------------------|
| 1.25 | 1360 | 2.5 | 1020 |
| 1.5 | 1330 | 2.75 | 976 |
| 1.75 | 1222 | 3 | 912 |
| 2 | 1140 | 3.25 | 838 |
| 2.25 | 1122 | 3.5 | 800 |

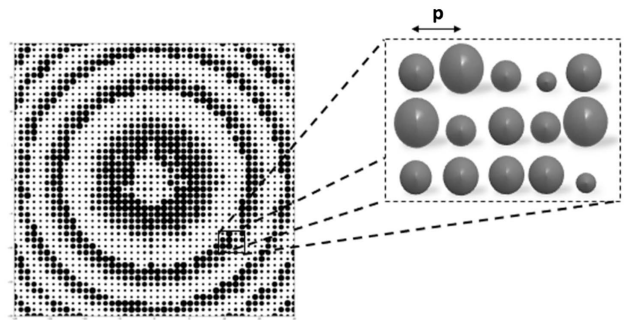


Fig. 4. Final radii distribution of a metalens using the inverse design method. Spheres are arranged in a square lattice with periodicity p . Radii of spheres are allowed to range from 150 nm to the half of the periodicity.

The FWHMs of the focal spots of the metalenses are shown in Fig. 5(a) as a function of the numerical aperture, where the solid black curve is the FWHM of a diffraction-limited spot of a lens with the given geometric parameters. Like the forward design method, there is no appreciable difference in the FWHM across the range of simulated indices, except at $n = 1.25$, where the FWHM does not decrease at very high numerical apertures. At lower numerical apertures, however, we observe

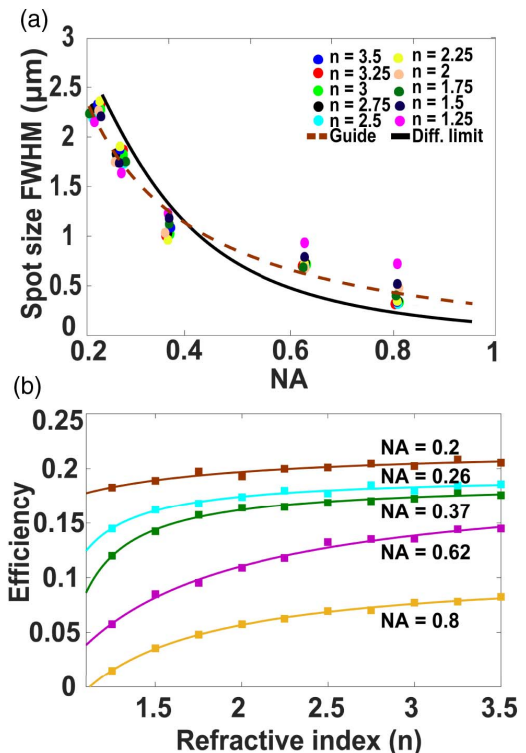


Fig. 5. Performance of the metalens using the inverse design method. (a) The FWHM of the focal spot as a function of numerical aperture of the lens. The solid and dashed curves are the diffraction-limited FWHM and guide to the eye, respectively. (b) The focusing efficiencies of metalenses with different numerical apertures against material refractive indices in the 1.25–3.5 range using the inverse design method. Different numerical apertures are specified with different colors, and plotted curves are guides to the eye.

that FWHMs are smaller than those of a diffracted-limited spot. We emphasize that this is not truly breaking the diffraction limit, but rather we attribute this to a larger proportion of the light intensity being located within side lobes as opposed to within the central peak. By shifting power from the central peak to the side lobes, beam spot sizes that are less than the diffraction-limited spot size are possible [35]. This shifting of light to the side lobes may have arisen from the defined figure of merit, in which we did not enforce a condition on the beam spot size and side lobe intensity ratio. The efficiencies of these metalenses are plotted as a function of their refractive indices in Fig. 5(b), where the different numerical apertures are specified with different colors. We find that the focusing efficiency decreases with increasing numerical aperture. According to Fig. 5(b), there is no significant difference in the focusing efficiency of high and low refractive index materials for low numerical apertures in the range of $NA = 0.2\text{--}0.37$ (50–100 μm focal length). For longer numerical apertures, however, such as 0.62 and 0.8, larger refractive index materials provide higher focusing efficiency.

4. DISCUSSION

A consistent behavior is observed between forward design (Fig. 3) and inverse design (Fig. 5) regarding the relation between the focusing efficiency of metalenses and their refractive index. For lower numerical apertures, there is no significant difference in the focusing efficiency of metalenses with refractive indices ranging from 1.25 to 3.5. However, for higher numerical apertures, achieving higher focusing efficiency metalenses is feasible by increasing their refractive index.

On the other hand, focusing efficiencies for metalenses with different numerical apertures using the inverse design method are much smaller than the ones in the forward design method. To understand why we have such a reduction in focusing efficiency, we calculated the transmission phase and amplitude of the spherical scatterers as a function of duty cycle (d/p) for SiN as a sample material, assuming a periodic boundary condition (Fig. 6) and found that they cannot provide a full 0-to- 2π phase shift range under varying diameters of the sphere, while maintaining a high transmission amplitude. As these spheres are the main building block of metalenses in the

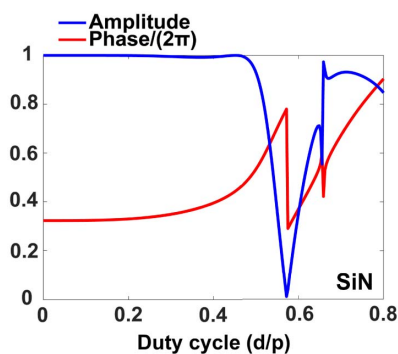


Fig. 6. Amplitude and phase of the transmitted light through a spherical scatterer: using RCWA, we calculate the transmission properties (red, phase delay; blue, transmission amplitude) as a function of the ratio of the sphere diameter and periodicity.

inverse design method, we cannot achieve high focusing efficiency for metalenses based on spherical scatterers. However, these results show that the same trend between forward design (Fig. 3) and inverse design (Fig. 5) regarding the relation between the focusing efficiency of the metalenses with the refractive index is not due to the actual phase or scatterer geometry, but is inherently dependent on the refractive index. Also, the FWHM of the focal spots from the inverse design method are smaller than those in the forward design method. We attribute this to our choice of figure of merit, for which we did not enforce a condition on the beam spot size.

The performance of a metalens is related to that of a metasurface beam deflector, which performance as a function of the material refractive index was recently analyzed at optical frequencies [17]. It was shown that while an efficiency greater than 80% can be obtained using high-contrast materials such as Si and Ge, for large-angle ($> 60^\circ$) beam deflection, the efficiency drops quickly for low-index materials, such as SiN. However, no significant difference in efficiency for modest deflection angles ($< 40^\circ$) was observed for different materials. Such behavior is justified by the coupled Bloch-mode analysis [17,36]. This finding is consistent with our result that for high numerical aperture metalenses, higher refractive index materials provide higher efficiency, but that at low numerical apertures, there is no significant difference in performance.

5. CONCLUSION

We have evaluated low-loss dielectric materials with a wide range of refractive indices for designing metalenses using both forward and inverse design methodologies. We found reasonable agreement between both methods in terms of the focusing efficiency and the FWHM of the focal spots on the material refractive indices. We found that for low numerical apertures ($NA < 0.6$), the efficiency of the metalenses is almost independent of the refractive index. For higher numerical apertures, however, high-index materials provide higher efficiency. The relationship between the refractive index and the metalens performance is significant in choosing an appropriate material, based on considerations such as ease and scalability of manufacturing, or a better tunability. In addition, we show that even with a very low refractive index ($n < 2$), we can achieve reasonable efficiency in a metalens, which will be significant for enabling fabrication with printable photonics technologies.

APPENDIX A

The intensity profile of an ideal lens with a focal length f and radius a is given by the Airy disk [37]:

$$I(\theta) = I_o \left(\frac{2J_1(ka \sin \theta)}{ka \sin \theta} \right)^2,$$

where I_o is the maximum intensity of the central peak, J_1 is the first order Bessel function of the first kind, k is the free space wave vector of incident light, and θ is the angular position from the focal point. In this paper, the diffraction-limited FWHM for a lens is calculated by fitting a Gaussian function (black curve) to the Airy disk, as shown in Fig. 7(a). In addition, we compared the diffraction limit using both approaches (Abbe diffraction limit and diffraction limit calculated by a Gaussian

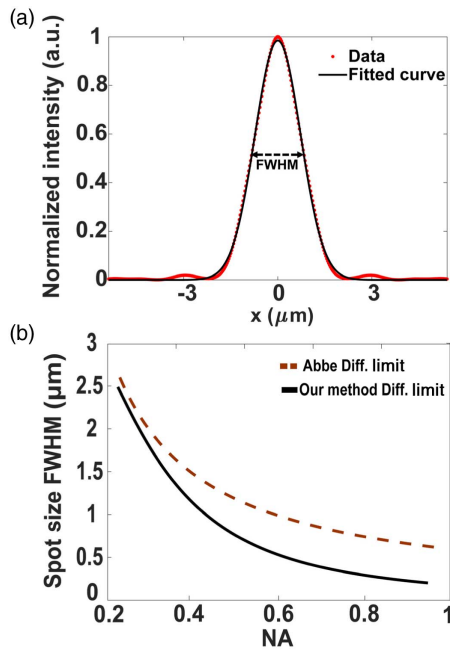


Fig. 7. (a) Example of a Gaussian fit to an Airy disk, which is generated by an ideal lens under the illumination by 1550 nm with a focal length of 50 μm and a radius of 40 μm . (b) The diffraction-limited FWHM of the focal spot as a function of numerical aperture of the lens. The dashed curve is the diffraction-limited FWHM using the Abbe diffraction limit approximation, and the solid curve is the diffraction limit calculated by a Gaussian fit to an Airy disk.

fit to an Airy disk) in Fig. 7(b). As it is shown in the Fig. 7(b), for high numerical apertures, our method provides a significantly smaller diffraction-limited FWHM.

Funding. Samsung; Global Research Outreach; University of Washington Reality Lab, Facebook, Google, and Huawei.

Acknowledgment. We thank the NVIDIA corporation for the contribution of the GPU for our calculations in the inverse design method. In addition, we thank Amos Egel, Lorenzo Pattelli, and Giacomo Mazzamuto for allowing us to use and further contribute to CELES.

REFERENCES

- N. Yu and F. Capasso, "Flat optics with designer metasurfaces," *Nat. Mater.* **13**, 139–150 (2014).
- S. Vo, D. Fattal, W. V. Sorin, Z. Peng, T. Tran, M. Fiorentino, and R. G. Beausoleil, "Sub-wavelength grating lenses with a twist," *IEEE Photon. Technol. Lett.* **26**, 1375–1378 (2014).
- A. Arbabi, Y. Horie, A. J. Ball, M. Bagheri, and A. Faraon, "Subwavelength-thick lenses with high numerical apertures and large efficiency based on high-contrast transmitarrays," *Nat. Commun.* **6**, 7069 (2015).
- D. Fattal, J. Li, Z. Peng, M. Fiorentino, and R. G. Beausoleil, "Flat dielectric grating reflectors with focusing abilities," *Nat. Photonics* **4**, 466–470 (2010).
- Y. Yang, W. Wang, P. Moitra, I. I. Kravchenko, D. P. Briggs, and J. Valentine, "Dielectric meta-reflectarray for broadband linear polarization conversion and optical vortex generation," *Nano Lett.* **14**, 1394–1399 (2014).
- G. Li, M. Kang, S. Chen, S. Zhang, E. Y.-B. Pun, K. W. Cheah, and J. Li, "Spin-enabled plasmonic metasurfaces for manipulating orbital angular momentum of light," *Nano Lett.* **13**, 4148–4151 (2013).
- G. Zheng, H. Mühlenbernd, M. Kenney, G. Li, T. Zentgraf, and S. Zhang, "Metasurface holograms reaching 80% efficiency," *Nat. Nanotechnol.* **10**, 308–312 (2015).
- X. Ni, A. V. Kildishev, and V. M. Shalaev, "Metasurface holograms for visible light," *Nat. Commun.* **4**, 2807 (2013).
- N. Yu, F. Aieta, P. Genevet, M. A. Kats, Z. Gaburro, and F. Capasso, "A broadband, background-free quarter-wave plate based on plasmonic metasurfaces," *Nano Lett.* **12**, 6328–6333 (2012).
- A. Arbabi, Y. Horie, M. Bagheri, and A. Faraon, "Dielectric metasurfaces for complete control of phase and polarization with subwavelength spatial resolution and high transmission," *Nat. Nanotechnol.* **10**, 937–943 (2015).
- A. Zhan, S. Colburn, C. M. Dodson, and A. Majumdar, "Metasurface freeform nanophotonics," *Sci. Rep.* **7**, 1673 (2017).
- M. Khorasaninejad, W. T. Chen, A. Y. Zhu, J. Oh, R. C. Devlin, C. Roques-Carmes, I. Mishra, and F. Capasso, "Visible wavelength planar metalenses based on titanium dioxide," *IEEE J. Sel. Top. Quantum Electron.* **23**, 43–58 (2017).
- Z. Wang, S. He, Q. Liu, and W. Wang, "Visible light metasurfaces based on gallium nitride high contrast gratings," *Opt. Commun.* **367**, 144–148 (2016).
- A. Zhan, S. Colburn, R. Trivedi, T. K. Fryett, C. M. Dodson, and A. Majumdar, "Low-contrast dielectric metasurface optics," *ACS Photon.* **3**, 209–214 (2016).
- S. Colburn, A. Zhan, E. Bayati, J. Whitehead, A. Ryou, L. Huang, and A. Majumdar, "Broadband transparent and CMOS-compatible flat optics with silicon nitride metasurfaces," *Opt. Mater. Express* **8**, 2330–2344 (2018).
- R. R. Reddy and Y. N. Ahammed, "A study on the Moss relation," *Inf. Phys. Technol.* **36**, 825–830 (1995).
- J. Yang and J. A. Fan, "Analysis of material selection on dielectric metasurface performance," *Opt. Express* **25**, 23899–23909 (2017).
- P. Lalanne and P. Chavel, "Metalenses at visible wavelengths: past, present, perspectives," *Laser Photon. Rev.* **11**, 1600295 (2017).
- H. Liang, Q. Lin, X. Xie, Q. Sun, Y. Wang, L. Zhou, L. Liu, X. Yu, J. Zhou, T. F. Krauss, and J. Li, "Ultrahigh numerical aperture metalens at visible wavelengths," *Nano Lett.* **18**, 4460–4466 (2018).
- R. Paniagua-Dominguez, Y. F. Yu, E. Khaidarov, S. Choi, V. Leong, R. M. Bakker, X. Liang, Y. H. Fu, V. Valuckas, L. A. Krivitsky, and A. I. Kuznetsov, "A metalens with a near-unity numerical aperture," *Nano Lett.* **18**, 2124–2132 (2018).
- F. A. Jenkins and H. E. White, *Fundamentals of Optics* (McGraw-Hill Education, 1937).
- F. T. Chen and H. G. Craighead, "Diffractive phase elements based on two-dimensional artificial dielectrics," *Opt. Lett.* **20**, 121–123 (1995).
- R. Søndergaard, M. Hösel, D. Angmo, T. T. Larsen-Olsen, and F. C. Krebs, "Roll-to-roll fabrication of polymer solar cells," *Mater. Today* **15** (1–2), 36–49 (2012).
- F. T. Chen and H. G. Craighead, "Diffractive lens fabricated with mostly zeroth-order gratings," *Opt. Lett.* **21**, 177–179 (1996).
- V. Liu and S. Fan, "S4: a free electromagnetic solver for layered periodic structures," *Comput. Phys. Commun.* **183**, 2233–2244 (2012).
- A. Zhan, T. K. Fryett, S. Colburn, and A. Majumdar, "Inverse design of optical elements based on arrays of dielectric spheres," *Appl. Opt.* **57**, 1437–1446 (2018).
- W. Stork, N. Streibl, H. Haidner, and P. Kipfer, "Artificial distributed-index media fabricated by zero-order gratings," *Opt. Lett.* **16**, 1921–1923 (1991).
- D. Rosenblatt, A. Sharon, and A. A. Friesem, "Resonant grating waveguide structures," *IEEE J. Quantum Electron.* **33**, 2038–2059 (1997).
- D. Sell, J. Yang, S. Doshay, R. Yang, and J. A. Fan, "Large-angle, multifunctional metagratings based on freeform multimode geometries," *Nano Lett.* **17**, 3752–3757 (2017).
- K. Wang, J. Zhao, Q. Cheng, and T. J. Cui, "Broadband and broad-angle low-scattering metasurface based on hybrid optimization algorithm," *Sci. Rep.* **4**, 5935 (2014).
- F. Aieta, M. A. Kats, P. Genevet, and F. Capasso, "Multiwavelength achromatic metasurfaces by dispersive phase compensation," *Science* **347**, 1342–1345 (2015).
- R. Pestourie, C. Pérez-Arancibia, Z. Lin, W. Shin, F. Capasso, and S. G. Johnson, "Inverse design of large-area metasurfaces," *Opt. Express* **26**, 33732–33747 (2018).

33. D. W. Mackowski and M. I. Mishchenko, "Calculation of the T matrix and the scattering matrix for ensembles of spheres," *J. Opt. Soc. Am. A* **13**, 2266–2278 (1996).
34. A. Egel, L. Pattelli, G. Mazzamuto, D. S. Wiersma, and U. Lemmer, "CELES: CUDA-accelerated simulation of electromagnetic scattering by large ensembles of spheres," *J. Quant. Spectrosc. Radiat. Transfer* **199**, 103–110 (2017).
35. A. A. Maznev and O. B. Wright, "Upholding the diffraction limit in the focusing of light and sound," *Wave Motion* **68**, 182–189 (2017).
36. J. Yang, D. Sell, and J. A. Fan, "Freeform metagratings based on complex light scattering dynamics for extreme, high efficiency beam steering," *Ann. Phys.* **530**, 1700302 (2018).
37. T. D. Gerke and R. Piestun, "Aperiodic volume optics," *Nat. Photonics* **4**, 188–193 (2010).